View Article Online / Journal Homepage / Table of Contents for this issue

Flexible morphology-controlled synthesis of mesoporous hierarchical α-Fe_2O_3 architectures and their gas-sensing properties

Quanyi Hao, Shuang Liu, Xiaoming Yin, Zhifeng Du, Ming Zhang, Limiao Li, Yanguo Wang, Taihong Wang* and Quihong Li*

Received 11th May 2010, Accepted 19th August 2010
DOI: 10.1039/c0ce00194e

Published on 06 October 2010. Downloaded by Michigan State University on 19/01/2016 20:57:19.

Mesoporous flower-like and urchin-like α-Fe_2O_3 nanostructures have been successfully synthesized by a simple solution-based reaction and sequential calcination. Detailed experiments demonstrated that the morphology of the hierarchical α-FeOOH precursors could be easily controlled by adjusting the experimental conditions including reactant concentration, solvent composition, reaction time, and reaction temperature. On the basis of time-dependent experiments, a multistage growth mechanism for the formation of the α-FeOOH super-architectures was proposed. In addition, by virtue of the unique hierarchical mesoporous structure and comparative high specific surface area, these obtained α-Fe_2O_3 nanostructures exhibited enhanced sensing performances to ethanol. This method is expected to be a useful technique for controlling the diverse morphologies of iron oxide superstructures that could meet the demands of a variety of applications, such as gas sensors, lithium-ion batteries, catalysis, waste-water treatment, and pigments.

1. Introduction

In recent years nanostructured materials have attracted considerable attention owing to their unique size, shape, and morphology-dependent fascinating properties that drastically differ from their bulk counterparts.[1–3] Consequently, researches on the shape- and morphology-controllable synthesis of nanomaterials are of great interest and actively being pursued. In particular, much efforts have been devoted to rational and skilful control of hierarchical and complex nanostructures self-assembled with low-dimensional building blocks (nanoparticles, nanorods, nanowires, nanosheets, *etc.*), due to their robustness, high specific surface area, and potential applications in catalysis,[4–6] drug delivery,[7] environmental abatement,[3,8,9] energy storage,[10–13] and sensors.[14–18] Inspired by these interests, many types of hierarchical superstructures with various morphologies (*e.g.*, aeroplanes,[19] flowers,[8,20] cages,[21] snowflakes,[22] dendrites,[23,24] and so on) have been successfully fabricated by a variety of methods, including soft/hard template-assisted route hydrothermal reaction, and sol–gel process. However, these methods usually hold disadvantages related to expensive surfactants and tedious synthetic procedures. The simplest route to prepare 3D hierarchical structures is generally considered to be a self-assembly process.[3] Nevertheless in spite of extensive research efforts, it is still a tremendous challenge due to the difficulty in control of nucleation and growth process.

Haematite (α-Fe_2O_3), exhibits n-type semiconducting properties with an indirect band gap of 2.2 eV, is the most stable iron oxide under ambient condition. It has been extensively used in diverse fields such as catalysis, chemical sensors, magnetic devices, electrode materials, and pigments, due to its low cost, high resistance to corrosion, environmentally friendly and fascinating physicochemical properties. Stimulated by these intriguing properties and broad applications, a wide variety of morphological α-Fe_2O_3 nanostructures, such as 0D (nanoparticles),[25] 1D (nanorods, nanowires, nanofibers, and nanotubes),[26–32] 2D/3D (nanosheets, nanodisks, nanospheres),[33–36] have been synthesized. However, only very recently, some hierarchically structured α-Fe_2O_3 with different shapes and morphologies have been reported, and showed promising potential applications in various fields.[8,11,17,19,22,23,37–41] For example, Gou *et al.*[39] have synthesized flutelike and branched porous haematite nanostructures through hydrothermal reaction, which exhibited unusual magnetic behaviour and good sensing performances towards ethanol. Zhong *et al.*[8] reported the synthesis of novel 3D flower-like iron oxide nanostructures with an excellent ability to remove various water pollutants. Studies by Cao *et al.*[22] Hu *et al.*[23] and Gu *et al.*[24] about α-Fe_2O_3 micron-pine dendrites have systematically investigated the formation mechanism and the effect of experimental conditions on the morphology. Unfortunately, these reported strategies for preparing hierarchically structured α-Fe_2O_3 are too tedious to large scale preparation due to the use of special equipment, high temperature/pressure, and soft/hard template. Consequently, designing a facile, economical, and effective route for controlled synthesis of self-assembled hierarchical iron oxide architectures is of great significance from the viewpoint of both fundamental research and practical application.

Herein, we propose a fast and facile solution-based route to simultaneously synthesize hierarchical α-FeOOH precursors without any templates at low temperature. We systematically investigated the effect of experimental conditions on the morphology of the α-FeOOH precursors, and the reaction mechanism for the formation of the hierarchical α-FeOOH architectures was studied. In addition, mesoporous α-Fe_2O_3

Key Laboratory for Micro-Nano Optoelectronic Devices of Ministry of Education, and, State Key Laboratory for Chemo/Biosensing and Chemometrics, Hunan University, Changsha, 410082, China. E-mail: thwang@hnu.cn; liquihong2004@hotmail.com; Fax: +86 0731 88823407; Tel: +86 0731 88823407

 This journal is © The Royal Society of Chemistry 2011

View Article Online

Published on 06 October 2010. Downloaded by Michigan State University on 19/01/2016 20:57:19.

superstructures have been successfully obtained by calcining the corresponding α-FeOOH precursors while preserving their original morphologies. The gas-sensing results demonstrated that these hierarchical α-Fe_2O_3 nanostructures showed enhanced response to ethanol. The present work is expected to gives a new insight into the easy and effective development of iron oxide super-nanostructures, and enhances the prospects for applications in a wide range of scientific and technological fields.

2. Experimental

2.1 Synthesis

All the chemicals were of analytical grade reagents and distilled water was used throughout the experiments. Hierarchical α-FeOOH precursors with different morphology were firstly synthesized using a solution-based method. In a typical procedure, 1.39 g of $FeSO_4 \cdot 7H_2O$ and 1.36 g of $CH_3COONa \cdot 4H_2O$ were dissolved in 50 mL of deionized water by ultrasonication at room temperature. After stirred vigorously in a water bath for a period at a given temperature of 40 or 60 °C, the yellow slurry was centrifuged and washed several times with distilled water and absolute alcohol, and finally dried at 70 °C, then flower-like or urchin-like α-FeOOH precursors were obtained. Further experiments were also conducted under different conditions, using procedures similar to that presented above. The final products of mesoporous hierarchical α-Fe_2O_3 architectures were obtained by calcining the as-prepared α-FeOOH precursors at 500 °C for 3 h in air.

2.2 Characterization

The crystal structure of the products were determined by X-ray diffraction (XRD, Siemens D-5000) with Cu-Kα ($\lambda = 1.5418$ Å). Scanning electron microscopy (SEM) images were performed on a Hitachi S-4800 microscope. Transmission electron microscopy (TEM) images, high-resolution transmission electron microscopy (HRTEM) images and selected area electron diffraction patterns (SAED) were taken on JEOL2010 electron microscope with an accelerating voltage of 200 kV. Measurement of specific surface area and analysis of porosity for the α-Fe_2O_3 products were performed through measuring Nitrogen adsorption–desorption isotherms with a Micromeritics ASAP2020 apparatus.

2.3 Sensor performance measurements

The fabrication and testing principle of the gas sensor are similar to that described in our previous reports.[16] Firstly, the α-Fe_2O_3 samples were mixed with terpineol to form a paste and then coated onto the outside surface of an alumina tube with a diameter of 1 mm and length of 4 mm. A Ni–Cr alloy coil through the tube was employed as a heater to control the operating temperature. To improve their stability and repeatability, the gas sensors were sintered at 300 °C for 10 days in air. Here, the sensing properties of the sensors were measured by a HW-30A gas-sensing measurement system (HanWei Electronics Co., Ltd., Henan, China) at a working temperature of 250 °C and 45% relative humidity (RH). The response and recovery time was the time required for a change of the output voltage to reach 90% of the equilibrium value after injecting and removing the detected gas, respectively.

3. Results and discussion

3.1 Structure and morphology

The crystallinity and phase information of the precursors and the final products have been confirmed with the X-ray diffraction (XRD) measurements. Fig. 1a and b are the XRD patterns of the flower-like and urchin-like α-FeOOH precursors that prepared at 40 and 60 °C, where all the diffraction peaks can be indexed to pure orthorhombic α-FeOOH with lattice constants $a = 4.616$ Å, $b = 9.955$ Å, and $c = 3.023$ Å (JCPDS 81-463). No characteristic peaks from impurities are observed. Part c and d of Fig. 1 are the XRD patterns of the final α-Fe_2O_3 products obtained by calcining the corresponding α-FeOOH precursors, all the diffraction peaks can be indexed as the hexagonal phase of α-Fe_2O_3 with lattice constants $a = 5.037$ Å, and $c = 13.77$ Å (JCPDS 89-596). The narrow and sharp peaks suggest that these α-Fe_2O_3 products are highly crystalline. No characteristic peaks are observed form impurities such as γ-Fe_2O_3, α-FeOOH and Fe_3O_4, indicating that these α-FeOOH precursors completely converted to α-Fe_2O_3.

The shape and morphology of the as-prepared samples were examined by scanning electron microscopy (SEM). Fig. 2a is the SEM image of the flower-like α-FeOOH precursors, which are composed of flower-like nanostructures with a diameter of about 1 μm. The magnified SEM image (insert of Fig. 2a) shows that the flower-like nanostructures are consisted of nanosheets with an average length of *ca.* 500 nm and a mean thickness of *ca.* 40 nm. The surface of the nanosheets is very smooth, probably due to Ostwald ripening.[8,42] Fig. 2c gives a representative SEM image of urchin-like α-FeOOH, and the samples are uniform urchin-shaped nanostructures with diameter of 1 μm, which consist of straight and radially grown nanorods. By careful observation (insert of Fig. 2c), we find that the nanorods with a diameter around 30–40 nm and length up to 500 nm radiate from the center. Parts b and d of Fig. 2 are the SEM images of the

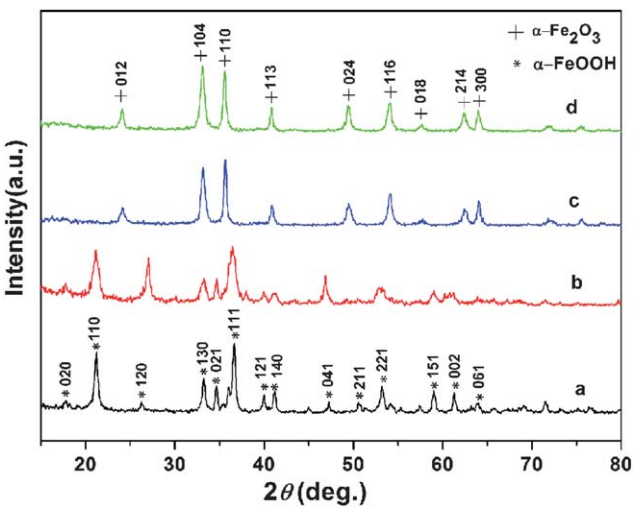

Fig. 1 XRD patterns of α-FeOOH (a: flower-like, b: urchin-like), and α-Fe_2O_3 super-architectures (c: flower-like, d: urchin-like).

View Article Online

Published on 06 October 2010. Downloaded by Michigan State University on 19/01/2016 20:57:19.

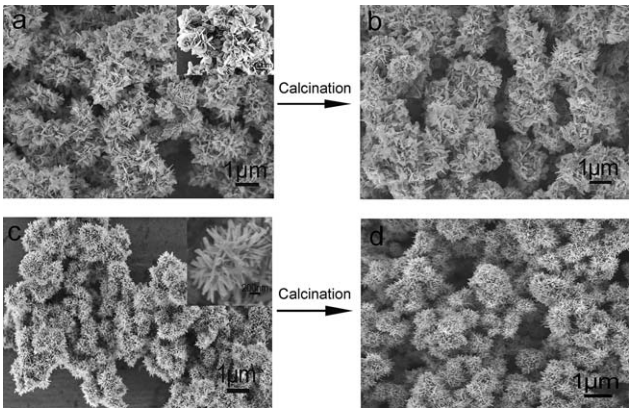

Fig. 2 SEM images of flower-like (a) and urchin-like(c) α-FeOOH (the insets are corresponding high magnification SEM images); (b) and (d) are the typical SEM images of flower-like and urchin-like α-Fe_2O_3 super-architectures.

flower-like and urchin-like α-Fe_2O_3 obtained by calcining the corresponding α-FeOOH precursors. These results show that the overall morphology and size of the flower-like and urchin-like structures are maintained after calcinations.

The morphology and microstructure of the samples were further investigated by transmission electron microscopy (TEM). Fig. 3a and 3d show the typical TEM images of the two different precursors, the flower-like and urchin-like morphologies can be observed clearly, which agree with the SEM results. Interestingly, a closer TEM observation of the flower-like structures further confirms that the building blocks are thin leaf-like nanosheets with nervure (inset of Fig. 3a). Fig. 3b and 3e show the detailed morphologies of these porous α-Fe_2O_3 nanostructures. It is worth noting that the morphologies were successfully maintained except that a lot of pores open to the outer surface and isolated from each other, which were probably due to the decomposition and re-crystallization of α-FeOOH and the release of large quantity of gases (dehydroxylation) during the calcinations process. The size of the pores distribution is less than 10 nm, which have been further confirmed by Brunauer–Emmett–Teller (BET) surface area and the pore size distribution analysis (Fig. 4). This hierarchical porous structure is believed to be an ideal host for gas sensing application.[14,15,39,43] Insets of Fig. 3b and 3e contain the SEAD patterns, which are taken from the whole areas of Fig. 3b and 3e, respectively. The diffraction rings indicate the high crystalline nature of the two α-Fe_2O_3 nanostructures. The lattice fringe spacing in the HRTEM image (Fig. 3c) taken from the nervure and vane of single leaf-like nanosheets in Fig. 3c are determined to be 0.27 nm, 0.37 nm, and 0.25 nm, corresponding to the (104), (012), and (110) *d*-spacing of the hexagonal α-Fe_2O_3, respectively. These lattice fringes taken from the nanorods of the urchin-like structures are clearly visible with a spacing of 0.37 nm (Fig. 3f), corresponding to the *d*-spacing of the (012) planes of α-Fe_2O_3. The clear lattice images demonstrate the high crystallinity and single-crystal feature of these α-Fe_2O_3 superstructures, which are in good agreement with the XRD and the SEAD results.

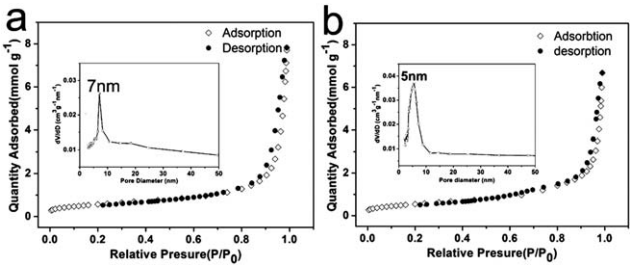

Fig. 4 Nitrogen adsorption–desorption isotherms and pore size distribution curves (insets) of flower-like (a) and urchin-like (b) α-Fe_2O_3 samples.

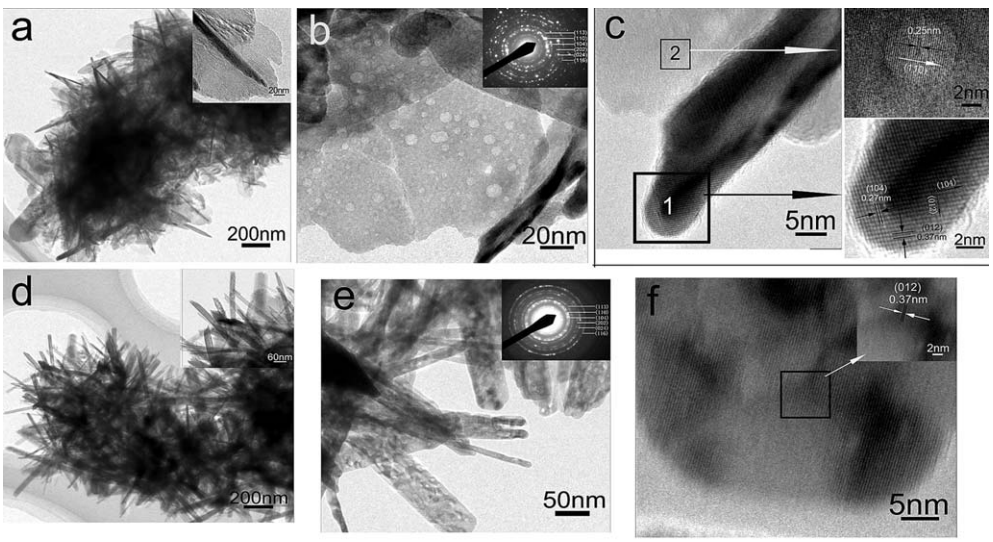

Fig. 3 (a) TEM image of the flower-like α-FeOOH (inset: the high-magnification image); (b) TEM image of the flower-like α-Fe_2O_3 (inset: the SAED pattern); (c) HRTEM image taken from single nanosheets; (d) TEM image of the urchin-like α-FeOOH (inset: the high-magnification image); (e) TEM image of the urchin-like α-Fe_2O_3 (inset: the SAED pattern); (f) HRTEM image taken from single nanorods.

 This journal is © The Royal Society of Chemistry 2011

View Article Online

Published on 06 October 2010. Downloaded by Michigan State University on 19/01/2016 20:57:19.

3.2 Effects of reaction conditions on the morphology of α-FeOOH precursors

Generally, the morphology and microstructure of nanocrystals vary greatly with the change of experimental parameters including reaction temperature, reactant concentration, surfactant, solvent, and solution pH value.[2,26,33] The present work mainly focused on the shape and morphology control of the α-FeOOH precursors by changing the reaction temperature, concentration of $CH_3COONa \cdot 4H_2O$, and volume ratio of the solvents.

The role of reaction temperature was found to be very critical in the morphology control. At room temperature (25 °C), densely structures consisted of irregular spindles with rough surface were formed (as shown in Fig. 5a). As the reaction temperature increased to 40 °C, the products had flower-like structures consisted of leaf-like nanosheets (Fig. 2a). It was interesting that, when the reaction temperature was increased to 50 °C, another flower-like structure assembled of leaf-like nanosheets and numerous small nanorods (Fig. 5b) could be obtained. As the reaction temperature was further increased to 60 °C, the as-formed products were composed of uniform urchin-like α-FeOOH superstructures assembled of nanorods radiating from the center (Fig. 2c). We proposed that the reaction temperature not only affected the nucleation and growth rates of particles but also might resulted in different adsorption ability of acetate ions (CH_3CHOO^-) on the different planes of α-FeOOH nuclei. Hence, increasing the reaction temperature may influence the nucleation and growth processes and facilitate the forming of nanorods. With further increase of the reaction temperature to 70 and 80 °C, the urchin-like α-FeOOH superstructures tended to be irregular, as shown in Fig. 4c and d.

The influence of CH_3CHOO^- on the morphology of α-FeOOH has also been investigated at the reaction temperature of 40 °C. Fig. 6a presents the typical SEM image of the α-FeOOH architectures obtained without $CH_3COONa \cdot 4H_2O$, while keeping other reaction conditions constant. It shows that the sample are small urchin-like architectures consisted of tiny nanorods. As the concentration of $CH_3COONa \cdot 4H_2O$ was increased to 0.34 g, irregular flower-like superstructures assembled of large nanosheets and many small nanorods were formed (Fig. 6b). When the concentrations reached 0.68 g, more interestingly, only a large quantity of leaf-like nanosheets densely and irregularly packed together (Fig. 6c). As 1.36 g of $CH_3COONa \cdot 4H_2O$ was added into the reaction solution, we synthesized the well developed flower-like α-FeOOH composed of leaf-like nanosheets (Fig. 2a). Based on the above results and previous reports,[28,35,40] we would like to point out that the morphologies of the products are closely related to the concentration of CH_3CHOO^-, which may favour the formation of the nanosheets and self-assembly of the flower-like α-FeOOH superstructures in the solution. This is probably due to the intrinsic anisotropic growth of goethite and the selective adsorption of CH_3CHOO^- at different faces. An intensive study is needed to substantially explore the more detailed formation mechanism of this phenomenon reported herein.

It is well known that the solvent is an important factor in the morphology evolution in solution-based strategies. Herein, the ethanol volume was also found to be responsible for the selective formation of α-FeOOH superstructures when other conditions were kept constant at 40 °C. From Fig. 7a–c, we can observe that the morphology of the final flower-like products became irregular and disorder with the increase of the ethanol volume from 5–10 mL and finally to 20 mL. It hints that the shape and morphology of the α-FeOOH superstructures can be influenced by adjusting the ethanol content in this reaction system.

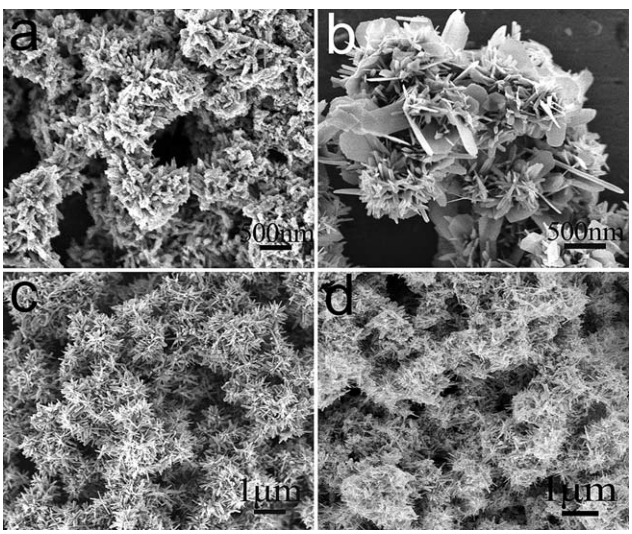

Fig. 5 SEM images of α-FeOOH prepared at different temperatures: (a) 25 °C; (b) 50 °C; (c) 70 °C; and (d) 80 °C.

3.3 Formation mechanism of hierarchical α-FeOOH precursors

In order to further understand the simultaneous synthesis and self-assembly process of the hierarchical α-FeOOH precursors, a series of time-dependent experiments were carried out. And the intermediate products obtained at different time intervals at given reaction temperatures were investigated by SEM for tracking morphological evolution (Fig. 8). As shown in Fig. 8a, under a short reaction time of 2 min at 40 °C, some few of tiny nanorods were obtained. After reaction for 10 min, undeveloped urchin-like superstructures consisted of small nanorods formed as a result of oriented attachment and self-assembly (Fig. 8b). When the reaction time was prolonged to 30 min, instead of the urchin-like congeries, the undeveloped flower-like α-FeOOH structures assembled of leaf-like nanosheets appeared (Fig. 8c), which was different from the previous reported mechanism for crystal growth in aqueous solution systems.[17,27,38,41,44,45] When the reaction time was further increased to 60 min, we got the fully developed flower-like superstructures as shown in Fig. 8d. It is worth noting that when the reaction temperature was set at 60 °C, the formation processes were somehow different from the procedure discussed above, and we obtained well-structured urchin-like α-FeOOH, as illustrated in Fig. 8e–h.

On the basis of the above experimental results and analysis, we proposed four major steps in the formation of the hierarchical α-FeOOH precursors as follows: (i) fast nucleation process; (ii) formation of the building blocks (nanorods) through aggregation; (iii) self-assembly of the nanorods to urchin-like superstructures through oriented attachment; (iv) recrystallization and

View Article Online

Published on 06 October 2010. Downloaded by Michigan State University on 19/01/2016 20:57:19.

Fig. 6 SEM images of α-FeOOH prepared with different $CH_3COONa \cdot 4H_2O$ concentrations: (a) 0 g; (b) 0.34 g; and (c) 0.68 g.

subsequent growth of the nanorods. This formation mechanism can be schematically depicted in Fig. 8.

$$CH_3COO^- + H_2O \rightarrow CH_3COOH + OH^- \quad (1)$$

$$4Fe^{2+} + 8OH^- + O_2 \rightarrow 4FeOOH + 2H_2O \quad (2)$$

First, in the initial stage, large numbers of primary α-FeOOH nanocrystals formed rapidly by the reaction of Fe^{2+} with O_2 and OH^- produced by the hydrolysis of CH_3COO^- as the eqn (1) and (2), which would serve as the nucleus in the following processes. In view of the primary particles formed through hydrolysis were thermodynamically unstable, many neighbouring primary nanoparticles further assembled into the rod-like building blocks with positive charged surface through oriented aggregation. As the reaction proceeded, the OH^- produced by the hydrolysis of CH_3COO^- increase, which neutralized the positive surface charge of the α-FeOOH nanorods, and led to the change of the surface charge. Due to the decrease of the surface charge, the nanorods interaction gradually evolved from repulsive to attractive, and the dispersive rod-like α-FeOOH nanocrystals tended to be self-assembled into quasi urchin-like superstructures through oriented attachment to reduce the surface energy. In the subsequent process, to further reduce the surface energy, the rod-like building units transformed into larger nanosheets related to a recrystallization also accompanied the "further growth" process, and the final fully developed flower-like α-FeOOH superstructures formed. An interesting finding was that the building blocks of the superstructures were quite different when the reaction temperature increased. When the reaction temperature changed to 60 °C, only well-structured urchin-like α-FeOOH comprised of nanorods obtained. All of these experimental results and analysis confirmed that the formation mechanism of these hierarchically structured α-FeOOH followed a self-assembled oriented attachment process, in which the initial formation of tiny crystalline nuclei was followed by crystal growth and self-assemble of the nanorods, and then recrystallization and subsequent growth of the nanorods driven by the minimization of overall surface energy. The results from such a process are similar to the flower-like iron oxide nanostructures in Zhong's work,[8] whereas the present low temperature self-assembling strategy is more simple and time-saving and facilitates the formation of nanostructures with high quality.

3.4 Gas-sensing performance of mesoporous α-Fe_2O_3 nanostructures

Our nitrogen adsorption–desorption analysis (Fig. 4a and inset) reveals that the specific surface area of the flower-like α-Fe_2O_3 nanostructures is about 46.9 $m^2\ g^{-1}$ and pore size distribution is centered at 7 nm. Similarly, as shown in Fig. 4b and inset, urchin-like α-Fe_2O_3 also shows mesoporous structural characteristics with specific surface area of about 45.0 $m^2\ g^{-1}$ and a monomodal pore distribution centered at 5 nm. Due to the comparative high specific surface area and mesoporosity, these nanostructured oxides might be advantageous for gas sensing application. Therefore, we investigated the sensing performance of these mesoporous α-Fe_2O_3 samples toward ethanol.

Fig. 10a plots the typical response characteristics towards ethanol of the sensors based on these as-synthesized flower-like (1) and urchin-like (2) mesoporous α-Fe_2O_3 nanostructures, and commercial α-Fe_2O_3 powder (3) at working temperature of 250 °C. Here, eight testing cycles corresponding to different ethanol concentrations from 1 to 500 ppm, respectively. As can be seen, voltage values increase abruptly upon the injection of ethanol, and then decrease rapidly to their initial value after the test gas is released. The response/recovery time of both designed α-Fe_2O_3 is less than 5/10 s, indicating fast respond and good reversibility. Moreover, the response magnitudes of both kinds hierarchical α-Fe_2O_3 improved dramatically with increasing the concentration of ethanol. Furthermore, the flower-like α-Fe_2O_3 showed better performance than the urchin-like α-Fe_2O_3 nanostructures when the gas concentration is higher than 30 ppm. It may be ascribed to the larger specific surface area and bigger pore, which would provide more accessible surface for the surface reaction.

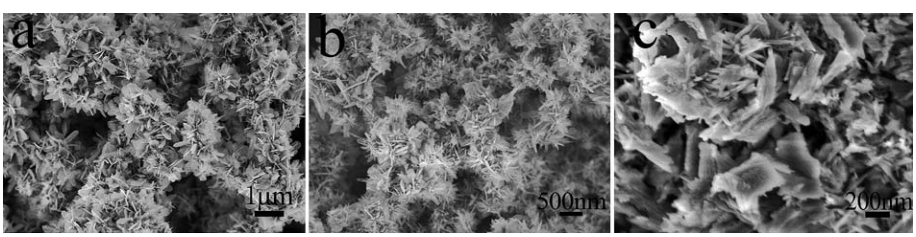

Fig. 7 SEM images of α-FeOOH prepared with different ethanol volumes: (a) 5 mL; (b) 10 mL; and (c) 20 mL.

 This journal is © The Royal Society of Chemistry 2011

View Article Online

Published on 06 October 2010. Downloaded by Michigan State University on 19/01/2016 20:57:19.

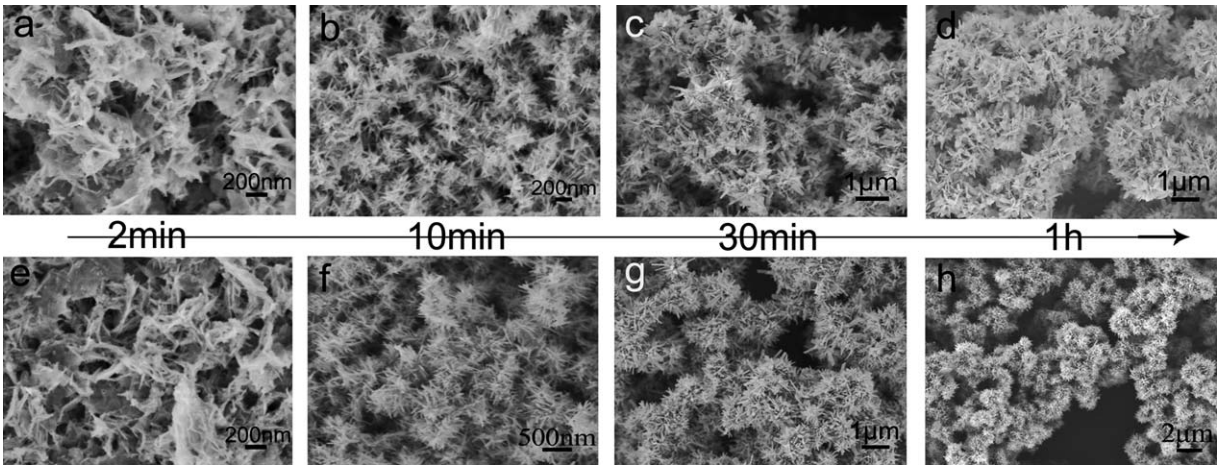

Fig. 8 SEM images of the flower-like (a–d) and urchin-like (e–f) α-FeOOH at different time intervals.

Compared with commercial powder, the responses of both kinds of α-Fe_2O_3 are greatly improved. The enhanced ethanol sensing properties could be attributed to the intrinsically comparative high specific surface areas and the unique hierarchical porous architecture, which can provide more adsorption–desorption active sites and facilitate the diffusion of the gas molecules and enable them to access all surfaces of the nanostructures.

Dynamic responsive curves are also shown in Fig. 10b, which shows a series of voltage responses of both kinds hierarchical α-Fe_2O_3 nanostructure-based sensors to dynamic switches between air and ethanol vapour. It is also found that the on and off responses for these products could be repeated several times without major changes, indicating the favorable stability and reversibility. These results indicate that the as-prepared hierarchical mesoporous α-Fe_2O_3 nanostructures are promising candidates for gas sensing application.

4. Conclusions

In summary, the present work demonstrated that hierarchical α-FeOOH precursors could be synthesized by a facile solution-based route without any templates at mild temperature. By adjusting the reaction temperature, flower-like and urchin-like nanostructures could be obtained. The effects of other reaction parameters on the α-FeOOH morphology were also systematically investigated. On the basis of the time-dependent experiments, a multistage reaction mechanism for the formation of the hierarchical α-FeOOH architectures was presented. The final mesoporous α-Fe_2O_3 nanostructures were successfully prepared by calcining the corresponding as-formed hierarchical α-FeOOH

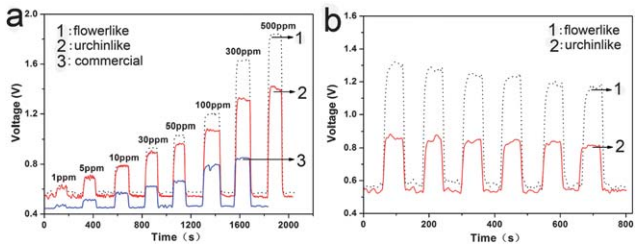

Fig. 10 (a) Typical response curves to ethanol vapour of gas sensors based on different α-Fe_2O_3 at 250 °C; (b) dynamic responsive curves of the mesoporous α-Fe_2O_3 to ethanol vapour of 50 ppm.

precursors. Due to their high specific surface and mesoporosity, these hierarchically mesoporous α-Fe_2O_3 nanostructures presented enhanced sensing responses to ethanol. It should be noted that the main feature is to propose a simple strategy to simultaneous synthesize iron oxides superstructures with tailored morphology. Furthermore, these obtained mesoporous hierarchical α-Fe_2O_3 nanostructures are also expected to be useful for other applications such as lithium-ion batteries, catalysis, wastewater treatment, and pigments.

Acknowledgements

This work was partly supported by "973" National Key Basic Research Program of China (grant no. 2007CB310500), National Natural Science Foundation of China (Grant No. 21003041), and Hunan Provincial Natural Science Foundation of China (Grant No.10JJ1011).

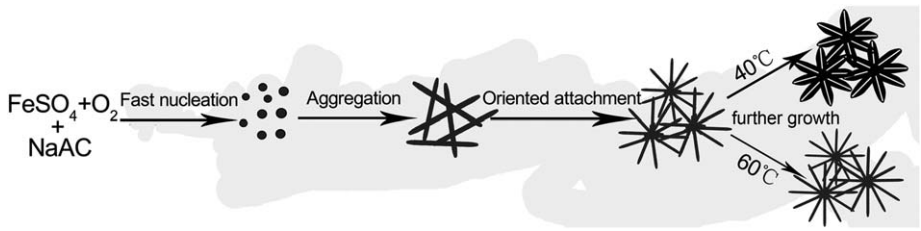

Fig. 9 Schematic illustrations for the growth process of the flower-like and urchin-like α-FeOOH prepared at 40 and 60 °C.

View Article Online

Published on 06 October 2010. Downloaded by Michigan State University on 19/01/2016 20:57:19.

References

1 C. Li, X. Yin, T. Wang and H. Zeng, *Chem. Mater.*, 2009, **21**, 4984–4992.
2 D. Wang, T. Xie and Y. Li, *Nano Res.*, 2009, **2**, 30–46.
3 J. Hu, L. Zhong, W. Song and L. Wan, *Adv. Mater.*, 2008, **20**, 2977–2982.
4 X. Song and L. Gao, *J. Phys. Chem. C*, 2008, **112**, 15299–15305.
5 X. Fu, J. Feng, H. Wang and K. Ng, *Nanotechnology*, 2009, **20**, 375601.
6 S. K. Mohapatra, S. E. John, S. Banerjee and M. Misra, *Chem. Mater.*, 2009, **21**, 3048–3055.
7 S. Liu, R. Xing, F. Lu, R. Rana and J. Zhu, *J. Phys. Chem. C*, 2009, **113**, 21042.
8 L. Zhong, J. Hu, H. Liang, A. Cao, W. Song and L. Wan, *Adv. Mater.*, 2006, **18**, 2426–2431.
9 J. Fei, Y. Cui, X. Yan, W. Qi, Y. Yang, K. Wang, Q. He and J. Li, *Adv. Mater.*, 2008, **20**, 452–456.
10 H. Wang, D. Qian, Z. Lu, Y. Li and R. Cheng, *J. Phys. Chem. Solids*, 2007, **68**, 1422–1427.
11 S. Zeng, K. Tang, T. Li, Z. Liang, D. Wang, Y. Wang, Y. Qi and W. Zhou, *J. Phys. Chem. C*, 2008, **112**, 4836–4843.
12 S. Liu, X. Yin, L. Chen, Q. Li and T. Wang, *Solid State Sci.*, 2010, **12**, 712–718.
13 P. Yu, X. Zhang, D. Wang, L. Wang and Y. Ma, *Cryst. Growth Des.*, 2009, **9**, 528–533.
14 J. Zhang, S. Wang, M. Xu, Y. Wang, B. Zhu, S. Zhang, W. Huang and S. Wu, *Cryst. Growth Des.*, 2009, **9**, 3532–3537.
15 X. Yin, C. Li, M. Zhang, Q. Hao, S. Liu, Q. Li, L. Chen and T. Wang, *Nanotechnology*, 2009, **20**, 455503.
16 C. Li, L. Li, Z. Du, H. Yu, Y. Xiang, Y. Li, Y. Cai and T. Wang, *Nanotechnology*, 2008, **19**, 35501–35501.
17 F. Zhang, H. Yang, X. Xie, L. Li, L. Zhang, J. Yu, H. Zhao and B. Liu, *Sens. Actuators, B*, 2009, **141**, 381.
18 F. Song, H. Su, J. Han, D. Zhang and Z. Chen, *Nanotechnology*, 2009, **20**, 495502.
19 S. Li, H. Zhang, J. Wu, X. Ma and D. Yang, *Cryst. Growth Des.*, 2006, **6**, 351–353.
20 L. Y. Chen, Z. D. Zhang and W. Z. Wang, *J. Phys. Chem. C*, 2008, **112**, 4117–4123.
21 J. Yu, X. Yu, B. Huang, X. Zhang and Y. Dai, *Cryst. Growth Des.*, 2009, **9**, 1474–1480.
22 M. Cao, T. Liu, S. Gao, G. Sun, X. Wu, C. Hu and Z. Wang, *Angew. Chem., Int. Ed.*, 2005, **44**, 4197–4201.
23 X. Hu, J. C. Yu and J. Gong, *J. Phys. Chem. C*, 111, pp. 11180–11185.
24 J. Gu, S. Li, E. Wang, Q. Li, G. Sun, R. Xu and H. Zhang, *J. Solid State Chem.*, 2009, **182**, 1265–1272.
25 T. Taniguchi, K. Nakagawa, T. Watanabe, N. Matsushita and M. Yoshimura, *J. Phys. Chem. C*, 2009, **113**, 839–843.
26 X. Hu and J. Yu, *Adv. Funct. Mater.*, 2008, **18**, 880–887.
27 B. Tang, G. Wang, L. Zhuo, J. Ge and L. Cui, *Inorg. Chem.*, 2006, **45**, 5196–5200.
28 J. Lian, X. Duan, J. Ma, P. Peng, T. Kim and W. Zheng, *ACS nano*, 2009, **3**, 3749–3761.
29 Z. Sun, X. Feng and W. Hou, *Nanotechnology*, 2007, **18**, 455607.
30 T. Almeida, M. Fay, Y. Zhu and P. Brown, *J. Phys. Chem. C*, 2009, **113**, 18689–139.
31 A. Nasibulin, S. Rackauskas, H. Jiang, Y. Tian, P. Mudimela, S. Shandakov, L. Nasibulina, S. Jani and E. Kauppinen, *Nano Res.*, 2009, **2**, 373–379.
32 K. Woo, H. Lee, J. Ahn and Y. Park, *Adv. Mater.*, 2003, **15**, 1761–1764.
33 M. Casula, Y. Jun, D. Zaziski, E. Chan, A. Corrias and A. Alivisatos, *J. Am. Chem. Soc.*, 2006, **128**, 1675.
34 N. Chaudhari, H. Kim, D. Son and J. Yu, *CrystEngComm*, 2009, **11**, 2264–2267.
35 C. Jia, L. Sun, F. Luo, X. Han, L. Heyderman, Z. Yan, C. Yan, K. Zheng, Z. Zhang and M. Takano, *J. Am. Chem. Soc.*, 2008, **130**, 16968–16977.
36 Z. Wu, M. Zhang, K. Yu, S. Zhang and Y. Xie, *Chem.–Eur. J.*, 2008, **14**, 5346–5352.
37 L. Zhang, J. Yu, Z. Zheng and C. Leung, *Chem. Commun.*, 2005, 2683–2685.
38 Z. An, J. Zhang, S. Pan and F. Yu, *J. Phys. Chem. C*, 2009, **113**, 8092–8096.
39 X. Gou, G. Wang, X. Kong, D. Wexler, J. Horvat, J. Yang and J. Park, *Chem.–Eur. J.*, 2008, **14**, 5996–6002.
40 S. Zeng, K. Tang, T. Li and Z. Liang, *J. Phys. Chem. C*, 2010, **114**, 274–283.
41 D. Du and M. Cao, *J. Phys. Chem. C*, 2008, **112**, 10754–10758.
42 Y. Cheng, Y. Wang, Y. Zheng and Y. Qin, *J. Phys. Chem. B*, 2005, **109**, 11548–11551.
43 M. Tiemann, *Chem.–Eur. J.*, 2007, **13**, 8376–8388.
44 L. Zhu, H. Xiao, X. Liu and S. Fu, *J. Mater. Chem.*, 2006, **16**, 1794–1797.
45 L. Zhu, H. Xiao and S. Fu, *Cryst. Growth Des.*, 2007, **7**, 177–182.

 This journal is © The Royal Society of Chemistry 2011